Depolarized light-scattering study of molten zinc chloride

M. J. Lebon,[1] C. Dreyfus,[1] G. Li,[2] A. Aouadi,[1] H. Z. Cummins,[1,2] and R. M. Pick[1]
[1]*Département de Recherches Physiques,* Université Pierre et Marie Curie, 4 Place Jussieu, 75252 Paris Cedex 05, France*
[2]*City College, City University of New York, New York, New York 10031*
(Received 16 September 1994)

Depolarized light-scattering experiments on molten $ZnCl_2$ have been performed in the frequency range 1–4000 GHz between 300 and 650 °C. The α relaxation was observed up to 650 °C. Comparison with mode coupling theory was attempted but gave inconclusive results due to the strong boson peak. The crossover temperature T_c was found to be in the range 270–310 °C. The thermal evolution of the boson peak in the liquid phase was followed up to 650 °C.

PACS number(s): 64.70.Pf, 78.35.+c

I. INTRODUCTION

Although the low-frequency light-scattering spectra of glass-forming liquids and their evolution with temperature through the glass transition have been the object of numerous studies, these spectra are still far from being completely understood. Recent experimental results obtained by neutron [1] and light-scattering [2] techniques have been reported to exhibit good overall agreement with the predictions of the mode coupling theory of the liquid-glass transition [3] for the thermal evolution of the density fluctuation correlation function of fragile glass formers. These studies have been very recently extended to other, less fragile, glass formers [4].

Among the molten salts, zinc chloride ($ZnCl_2$) is unusual from several points of view. It is one of the simplest glass formers and melts at a fairly low temperature (glass transition temperature $T_g = 102$ °C, melting temperature $T_m = 318$ °C). At the melting temperature, $ZnCl_2$ shows an unusually high viscosity [5], with low ionic mobility and conductivity [6]. Its viscosity curve as a function of T_g/T is very similar to that of SiO_2-Na_2O, which allows zinc chloride to be placed, in the Angell classification [7], as a glass former intermediate between strong glasses like SiO_2 and fragile glasses like CKN. In this sense, its behavior is similar to that of glycerol [4(a)].

$ZnCl_2$ has also been the object of numerous studies including extensive x-ray [8], neutron diffraction [9–11], and extended x-ray absorption fine-structure [12] experiments, which have shown that the structure of the glassy and molten phases is a distorted random close-packed structure of Cl^- anions providing tetrahedral sites occupied by the Zn^{2+} ions. The Zn^{2+} ions are arranged in such a way that the tetrahedral corner sharing of the cations is maximized. Dynamical properties have also been the object of numerous studies: vibrational Raman [13], infrared [14], and Brillouin [15,16] spectroscopies, longitudinal ultrasonic absorption, and shear relaxation measurements [17]. Also, results have been obtained recently just above T_g by photon correlation techniques [18].

In this paper we report a study of the depolarized light-scattering spectrum of this material in the molten phase and in the high temperature part of the supercooled phase. In spite of the small accessible temperature range of the latter because of unavoidable crystallization, the high viscosity of $ZnCl_2$ at a high temperature allows us to study phenomena usually only observed far into the supercooled phase.

The paper is organized as follows. Section II summarizes the results of mode coupling theory we wish to probe by our experiments and the most important aspects of light scattering in $ZnCl_2$. After a brief Sec. III giving some details on the experimental setup and on the way our frequency spectra were determined, Sec. IV proceeds to the analysis of those spectra in three specific frequency domains to be defined in Sec. II A. The results are finally discussed in Sec. V.

II. GENERAL BACKGROUND

A. Excitations in glasses and in glass-forming liquids

The main dynamical signature encountered during the glass transition is the so-called α relaxation, the characteristic relaxation time τ_α of which can be as small as 10^{-12} s in the supercooled phase close to T_m, and increases rapidly with decreasing temperature. This allows one to define the phenomenological glass temperature T_g as the temperature at which τ_α becomes longer than the characteristic time of thermodynamic measurements, typically 100 s. By performing neutron scattering experiments in fragile supercooled liquids, it has been recognized that, at high temperature, this α relaxation is actually the slowest part of a more complicated two-step relaxation process. This two-step process has been predicted by the mode coupling theory of the glass transition [3(c)], which will be discussed in Sec. II B.

Also, while it has been recognized for many years that the Raman spectrum of glasses generally exhibits a low-frequency maximum [or light-scattering excess (LSE) in short], the partial persistence of this maximum in the cor-

*Centre National de la Recherche Scientifique URA 71.

responding supercooled liquids [19] has only been noticed very recently. A correlation between the magnitude of this LSE and the fragility of the glass seems also to exist: the stronger the glass, the larger the intensity of the boson peak [20]; we shall return to the detailed structure of this peak in Sec. IV C.

The two steps of the relaxation process usually occur at lower frequencies than the LSE, though significant overlap may occur, as we shall see later. These two steps and the LSE are the three frequency regions we shall analyze in Sec. IV.

B. Mode coupling theory of the glass transition

Up to now, the only theoretical approach that can globally explain the low-frequency dynamics of liquids approaching the glass transition is the mode coupling theory (MCT) [21] of the glass transition [3]. This theory allows us to link these phenomena to the slow relaxation of the flow process.

The main variables considered in the MCT are the correlation functions of the density fluctuations

$$\phi_q(t)=\langle \delta\rho_q(t)\delta\rho_q(0)\rangle /S_q \ , \tag{2.1}$$

where $\delta\rho_q$ is the qth Fourier component of the microscopic density fluctuations and S_q is the static structure factor. In the Zwanzig-Mori theory of liquids, the density-fluctuation correlation functions can be expressed, in the Laplace transform space, by a set of continued fractions,

$$\phi_q(z)=-\{z-\Omega_q^2[z+M_q(z)]^{-1}\}^{-1} \ , \tag{2.2}$$

where Ω_q is a characteristic microscopic frequency scale and $M_q(z)$ is a memory function that can be understood as a generalized damping function. In mode coupling theories, the memory function is used to introduce retarded nonlinear couplings between the density-fluctuation correlation function $\phi_q(t)$ and the other dynamical variables of the fluid. At frequencies lower than the typical microscopic frequencies, the idealized MCT memory function can be expressed as

$$M_q(z)=i\nu_q+\Omega_q^2 m_q(z) \ , \tag{2.3}$$

where ν_q is a damping constant, while the function $m_q(t)$ couples $\phi_q(t)$ to products of all the other density-fluctuation functions. The coupling coefficients vary smoothly with the physical control parameters of the system (e.g., density and temperature) and it can be shown numerically that, as the coupling coefficients increase regularly with these control parameters, a singularity appears for $t\to\infty$ (i.e., for $z\to 0$) in the solutions of Eq. (2.2). This singularity takes place simultaneously for all wave vectors and, at constant pressure, where the sole control parameter is the temperature, this allows us to define a critical temperature T_c, which is higher than the usual calorimetric glass transition temperature T_g.

In the vicinity of T_c, and in a frequency range for which $(z+i\nu_q)/\Omega_q{}^2 \ll m_q(z)$, Götze and Sjögren [22] showed that the solutions of Eq. (2.2) exhibit scale invariance. The spectrum can be divided into two regions corresponding to two different frequency scales: the lower frequency range corresponds to the α process described above, which should obey some particular scaling laws; the higher frequency region is called the fast β-relaxation region. According to the idealized MCT, the complete behavior of the correlation functions in the fast β region and the frequency of the α process maximum are determined by a single mathematical control parameter σ and a system-dependent exponent parameter λ for all values of the wave vector $\mathbf{q}$. σ is the separation parameter given approximately by $\sigma=(T_c-T)/T_c$. The theoretical results related to Eq. (2.2) are usually expressed either directly by using the intermediate density-fluctuation correlation function $F(q,t)$, or through the dynamical structure factor $S(q,\omega)=\mathcal{F}[F(q,t)]$ and its associated susceptibility spectrum $\chi_q''(\omega)=\omega\,\mathrm{Re}\{S(q,\omega)\}$. In this paper, we shall only discuss susceptibility spectra.

For $T>T_c$, the MCT susceptibility spectra show a minimum, which is described by the interpolation formula

$$\chi_q''(\omega)=\chi_{q\,\min}''[b(\omega/\omega_{\min})^a+a(\omega_{\min}/\omega)^b]/(a+b) \ , \tag{2.4}$$

where $\chi_{q\,\min}''$ and $\omega_{\min}$ obey the power laws

$$\chi_{\min}''\propto(T-T_c)^{1/2} \ , \tag{2.5}$$

$$\omega_{\min}\propto(T-T_c)^{1/2a} \ . \tag{2.6}$$

The exponents a and b are not independent but are determined by the exponent parameter λ through the relation

$$\Gamma^2(1-a)/\Gamma(1-2a)=\Gamma^2(1+b)/\Gamma(1+2b)=\lambda \ , \tag{2.7}$$

$$\text{with } 0<a<0.395 \ , \quad 0<b<1 \ . \tag{2.8}$$

For the longer-time relaxation process (the α relaxation), which exists for $\omega\ll\omega_{\min}$, the relaxation time τ_α should obey another power law

$$\tau_\alpha\propto(T-T_c)^{-\gamma} \ , \quad \text{where } \gamma=1/2a+1/2b \ . \tag{2.9}$$

For $T<T_c$, the idealized MCT predicts a structural arrest, i.e., a nonzero $t\to\infty$ limit for $\phi_q(t)$ for all q, and the disappearance of the α relaxation. This is, of course, an unphysical result, since $T_c>T_g$ and the α relaxation persists at least down to T_g. A more realistic dynamics can be recovered if activated hopping processes are included in the memory function; those terms, which couple density fluctuations to currents, eliminate the structural arrest at T_c and smooth out the transition. This is done in the extended versions of MCT [23]. In this paper we shall consider only the results predicted by the idealized MCT, the new terms being unimportant for temperatures well above T_c.

C. Light-scattering mechanisms

As noted above, the MCT predicts the behavior of the dynamic structure factor $S(q,\omega)$. A direct experimental technique to measure $S(q,\omega)$ for nonzero wave vectors is provided by inelastic neutron scattering. The link between $S(q,\omega)$ and depolarized light-scattering experiments is less direct and will now be briefly discussed.

The low-frequency light-scattering spectrum of a fluid is related to the spectrum of the fluctuations of its polarizability tensor Π [24]. Two independent contributions can be defined:

$$I_{\rm iso}(\omega)=A\int dt\,\exp(-i\omega t)\langle\Pi_{\rm iso}(t)\Pi_{\rm iso}(0)\rangle\ , \tag{2.10}$$

$$I_{\rm ani}(\omega)=A\int dt\,\exp(-i\omega t)\langle\Pi_{\rm ani}(t)\Pi_{\rm ani}(0)\rangle\ , \tag{2.11}$$

where A is a constant determined by the experiment, and where $\Pi_{\rm iso}$ and $\Pi_{\rm ani}$ are the isotropic and anisotropic parts of the polarizability tensor, respectively.

In a complex fluid, a first contribution to $I_{\rm ani}$ is associated with the reorientation of any anisotropic molecule or ionomolecular entity [24]. While the ionic species present in molten $ZnCl_2$ are not entirely known, the main ionic species reported so far are Zn^{2+}, Cl^-, and $ZnCl_4^{2-}$. Since none of these has an anisotropic polarizability tensor, we shall assume that the depolarized light-scattering spectra do not come from orientational effects.

In one-component isotropic van der Waals liquids, the dominant process contributing to the depolarized light-scattering intensity is the dipole–induced-dipole (DID) mechanism [25], which contributes only to $\Pi_{\rm ani}$. In this mechanism, the polarization of a molecule by the laser beam polarizes the medium and is the source of $\Pi_{\rm ani}$; therefore $\Pi_{\rm ani}$ involves a two-particle density and the DID contribution to $I(\omega)$ involves a four-particle two-time density correlation function. Provided that a factorization assumption is made [26], the latter can be expressed as a product of two-particle correlation functions, as first proposed by Stephen [27]. The DID intensity becomes

$$\begin{aligned} I^{\rm DID}(\omega)&=\mathcal{F}\int d\mathbf{q}\,f^2(\mathbf{q})F^2(\mathbf{q},t)\\ &=\int\int d\mathbf{q}\,d\omega' f^2(\mathbf{q})S(\mathbf{q},\omega')S(-\mathbf{q},\omega-\omega')\ , \end{aligned} \tag{2.12}$$

where $\mathcal{F}$ stands for the Fourier transform and $f(\mathbf{q})$ is the Fourier transform of the trace of the dipole operator. Following MCT, $S(\mathbf{q},\omega)$ factorizes in the fast β-relaxation regime into a function of q multiplied by a function of ω. Taking into account the existence of a large low-frequency contribution to this function, it can be shown [28] that, for frequencies above the α peak, the light-scattering intensity, which appears as a large excess intensity above the intensity of the low-temperature glass, is proportional to $S(\mathbf{q},\omega)$. This relation has been used in several studies of the glass transition in organic or inorganic glasses [2,29].

Actually, the case of $ZnCl_2$ is more complex for two reasons. First, both Zn^{2+} and Cl^- can be polarized. Thus the DID $\Pi_{\rm ani}$ contains contributions from cations and anions and three kinds of correlation functions [$F^{\rm Cl\text{-}Cl}(q,t)$, $F^{\rm Cl\text{-}Zn}(q,t)$, and $F^{\rm Zn\text{-}Zn}(q,t)$] appear in the generalization of Eq. (2.12). Nevertheless, due to the respective polarizabilities and concentrations of Zn^{2+} and Cl^- ($\alpha^{Zn^{2+}}=5$ a.u., $\alpha^{Cl^-}=19$ a.u.) [30], only the anions yield a significant contribution to $I(\omega)$, i.e., only the intermediate scattering function $F^{\rm Cl\text{-}Cl}(q,t)$ is important. Second, other polarization mechanisms exist, which have also to be taken into account: the polarizibility of an ion can be directly influenced, e.g., by the Coulomb field created by the other ions, by the gradient of this Coulomb field, or by short-range overlap interactions [31]. The polarizability fluctuations should then be expressed as

$$\Pi=\Pi^{\rm DID}+\Pi^{\gamma}+\Pi^{B}+\Pi^{\rm SR}\ldots\ . \tag{2.13}$$

Depending on their nature, these terms contribute either to both the isotropic and the anisotropic light-scattering intensities (short-range, $\Pi^{\rm SR}$, and Coulomb field, Π^{γ}) or only to the anisotropic intensity (DID, $\Pi^{\rm DID}$, and Coulomb field gradient, Π^{B}). Also, cross-correlation contributions exist. The important point is that each term of Eq. (2.13) depends on the same two-particle density, so that, as in the case of a pure DID mechanism, the light-scattering intensity depends on that four-particle correlation function, which can be factorized within the Stephen approximation. In this case $F^{\rm Cl\text{-}Cl}(q,t)$ can be shown to be an important, if not the only, contribution. As the different contributions could have different weights in $\Pi_{\rm iso}$ and $\Pi_{\rm ani}$, and as they can describe different dynamics, one could expect the depolarization ratio

$$\rho(\omega)=I_{\rm ani}(\omega)/[I_{\rm iso}(\omega)+(4/3)I_{\rm ani}(\omega)] \tag{2.14}$$

to vary with frequency. Actually as described below, this is not the case for $ZnCl_2$; $\rho(\omega)$ is essentially constant and close to 0.5, which indicates that $I_{\rm iso}(\omega)$ is weaker than (but proportional to) $I_{\rm ani}(\omega)$, while the latter is dominated by its DID contribution. We conclude that the present experiment probes essentially the Cl^--Cl^- dynamics.

III. EXPERIMENT AND RESULTS

Samples of $ZnCl_2$ were prepared following the protocol given by Soltwitsch, Sukmanovski, and Quitmann [16], and kept in vacuum-sealed silica cells. A clear liquid was obtained, which was easily vitrified by quenching, whereas by cooling slowly, crystallization always occurred at about 280 °C.

Two different sets of experiments were performed. The Raman spectra were recorded at City College on a Spex 1401 double holographic grating spectrometer; the laser was a Spectra Physics Ar^+ laser, and the sample was placed in an Oxford oven.

The interferometric experiments were performed in Paris with a Sandercock-type tandem Fabry-Pérot interferometer [32], in the near backscattering depolarized geometry in order to minimize the longitudinal Brillouin lines and eliminate the transverse Brillouin lines at low temperature. Great care was taken in the control of the coupling between the two Fabry-Pérot étalons in order to get a good definition of the free spectral range, even at the smallest separation (0.22 mm). The experimental setup is shown in Fig. 1. Polarization of the scattered light was selected with a large aperture Glan-Taylor prism; an Amici prism and a variable size exit pinhole were used to adjust the spectral window of the scattered light. The

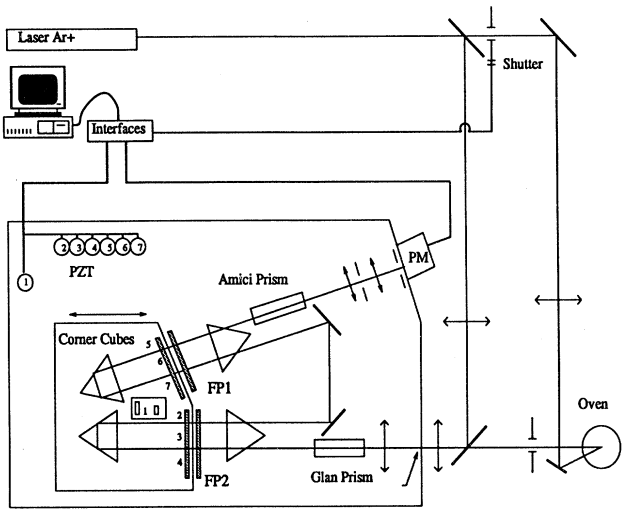

FIG. 1. Tandem Fabry-Pérot interferometer with experimental setup.

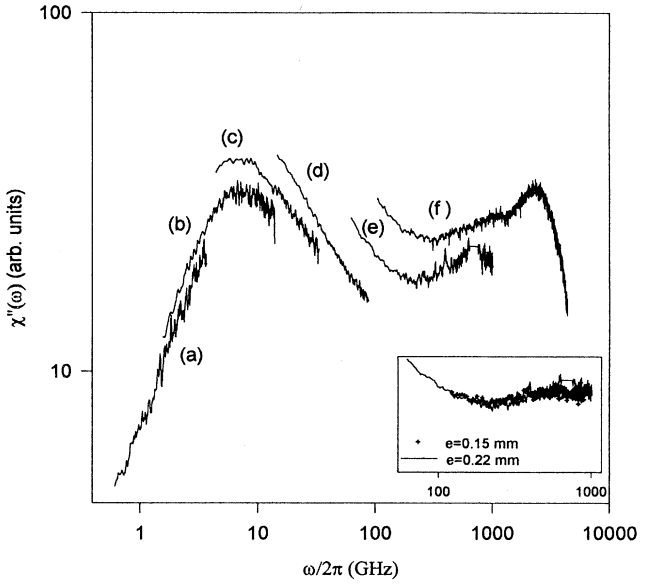

FIG. 2. $ZnCl_2$ susceptibility spectra at 600 °C: (a)–(e) are tandem Fabry-Pérot spectra and (f) is a Raman spectrum. Etalon spacings are (a) 26 mm, (b) 10 mm, (c) 3 mm, (d) 1 mm, and (e) 0.22 mm. Inset: 0.15 mm and 0.22 mm spacing spectra used to eliminate effects due to the ghost.

laser was an Innova-90 Coherent Ar^+ laser operated in single mode at 514.5 nm.

The oven, which was built in the Paris laboratory workshop, allows experiments to be performed up to 700 °C for several scattering angles. The temperature was kept constant within 1 °C during the experiments. We checked that the temperatures inside the sample cell and at the location of the temperature probe were the same to within 2 °C.

For each temperature, one Raman spectrum and five tandem Fabry-Pérot spectra were recorded. The main problems we encountered were the scaling of the six spectra at each temperature to obtain a composite spectrum, and the measurement of the relative intensities of these composite spectra at different temperatures. The scaling of the spectra is illustrated in Fig. 2, where the six susceptibility spectra at 600 °C are shown.

As can be seen, there is no ambiguity for these spectra in adjusting their intensity scales to obtain a composite total spectrum, except for the 0.22 mm spectrum (e), where the joining is disturbed by the presence of a ghost [32]. In the inset of Fig. 2 a spectrum recorded with a smaller étalon spacing allowed us to determine the relevant part of the spectrum. Such difficulty would have arisen if the recorded spectra were superimposed on an appreciable background of different origin. We minimized the background by taking great care in eliminating as much as possible the stray light coming from the sample and in matching correctly the exit pinhole with the free spectral range. The adjustment necessary to obtain a composite spectrum turned out to be possible over a large frequency range. However, we did encounter difficulties at the lowest temperatures for the lowest free spectral range, where a low signal-to-noise ratio could not be avoided. This is the reason why the frequency range of the susceptibility spectra at low temperatures is smaller than at higher temperatures.

In molecular compounds, the relative intensities of spectra recorded at different temperatures can be calibrated by using an internal vibration mode as an intensity reference [20,33]. This internal mode is recorded in the Raman spectra at the same time as the low-frequency part, so that the relative intensity of these Raman spectra is accurately known. This is not possible for $ZnCl_2$, in which there is no temperature-independent internal mode. We have therefore proceeded in the following way to estimate the relative intensities: between 1 and 15 cm^{-1}, we scanned a small section of the spectrum several times at each temperature, keeping the alignment of the reference beam as stable as possible and taking the integrated intensity of the reference beam as an external monitor. Inelastic scattered intensities recorded at the same temperature on three consecutive days showed a variation of approximately 10%, which we take as an estimate of the uncertainty in the relative intensities. However, the focal point of the incident beam inside the sample can vary during a temperature cycle without a change of the geometrical alignment; due to this effect, the uncertainty in relative intensities may exceed our estimate of 10%.

The depolarization ratio was measured at 325 °C for the Raman spectra by inserting a scrambler in the scattered light beam. Outside of the Brillouin lines, a similar measurement was made in the interferometric measurements between half-wave plates at 450 and 650 °C. In all cases, the value of the depolarization ratio was approximately 0.5 and was constant in the measured frequency range, as stated at the end of Sec. II C.

IV. ANALYSIS OF THE RESULTS

The complete set of composite spectra is plotted in Fig. 3. Figure 3(a) represents the reduced intensities

$$I_{\text{red}}(\omega)=I(\omega)/\omega[1+n(\omega)]\ , \tag{4.1}$$

where $n(\omega)$ is the Bose factor; the susceptibility spectra $\chi''(\omega)=\omega I_{\text{red}}(\omega)$ are shown in Fig. 3(b), where the three spectral regions discussed in Sec. II can be seen.

(i) At low frequency, a large peak is visible, the frequency of which decreases rapidly with decreasing temperature. At 650 °C, the high-frequency wing of this peak merges with the high-frequency structure. Conversely, this peak has disappeared below the frequency window of our spectrometer for $T<400$ °C. This peak is closely related to the structural or α-relaxation phenomenon and will be called hereafter the α peak. It has been seen previously by several experimental techniques [3(c)].

(ii) At intermediate frequencies, there is a minimum of the susceptibility, the frequency and magnitude of which decrease with decreasing temperature. This also has already been observed in other materials, in both light-scattering and neutron-scattering experiments [1,2].

(iii) At higher frequencies, the behavior of the susceptibility is more complex. One clearly sees at low temperature a broad peak, the low-frequency side of which becomes less and less apparent as the temperature increases, while its high-frequency side remains well defined whatever the temperature. This broad peak, also clearly visible in Fig. 3(a) is the LSE. Further analysis will show that this peak has two components. For reasons to be discussed later, we shall call the high-frequency component "microscopic peak" and the low-frequency one "boson peak." Let us consider successively these three spectral regions.

A. The α-peak region

The α peak is well separated from the other parts of the spectrum in the temperature range we studied, so that one can try to fit it by a function not related to the rest of the spectrum. This fit was made using a standard nonlinear least squares method for the optimization and either a Cole-Davidson function or a Debye function to represent the relaxation process in the frequency domain. The fits are shown in Fig. 4 and show good agreement only for the Cole-Davidson function. As already mentioned, for temperatures lower than 350 °C, no fit was possible because the α peak moved outside of the experimental frequency window. The β and τ parameters of the Cole-Davidson function found from the fit were then transformed into the corresponding β_K and τ_K of the stretched exponential (Kohlrausch or KWW function) using the result of [34]. The latter are shown in Figs. 5(a) and 5(b) and listed in Table I together with values derived from viscosity and acoustic measurements. In the whole range of temperatures where the fit was possible, β_K was found to be almost constant within the error bars. In

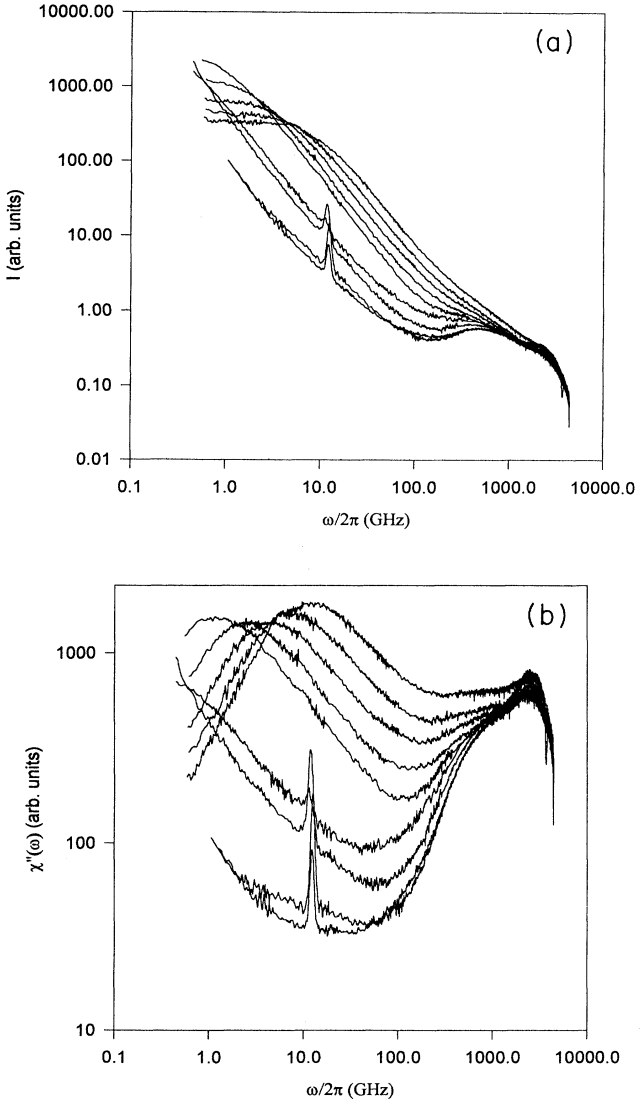

FIG. 3. (a) Reduced intensity spectra for (bottom to top) 300 °C, 350 °C, 400 °C, 450 °C, 500 °C, 550 °C, 600 °C, 650 °C. (b) Susceptibility spectra, temperatures as in (a).

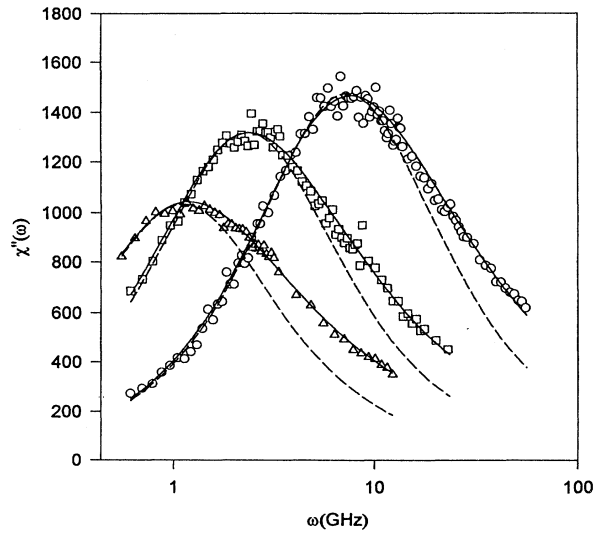

FIG. 4. Comparison of experimental α-relaxation susceptibility spectra with Debye (— — —) and Cole-Davidson (——) relaxation laws for $T=450$ °C (△), 500 °C (□), and 650 °C (○).

Fig. 5(a) we also show the parameter β_K determined at lower temperatures in a recent quasielastic light-scattering experiment (QELS) [18]. It can be seen that the variation of β_K, if any, is very weak, all the values being nearly identical in the whole supercooled phase and far inside the liquid phase. This is in contrast with recent results on fragile glasses [35], which have generally shown that β_K decreases with decreasing temperature below a certain temperature and is almost constant above this temperature.

The variation of τ_K is plotted on a logarithmic scale versus $(T-T_0)^{-1}$ where $T_0=1\,°C$ is a Vogel-Fulcher temperature [Fig. 5(b)]. Several values for T_0 can be found in the literature depending on the experimental method used [5]; they all yield $-23\,°C<T_0<7\,°C$. The relaxation times arising from the QELS experiment are also shown in Fig. 5(b) together with those determined from viscosity [5,6] and acoustic shear modulus measurements [17]. It can be seen that the time dependence of τ_K agrees very well with a Vogel-Fulcher law, the best fit giving $T_0=1\,°C$.

The variation of τ_K is also shown as an "Angell plot" in Fig. 5(c), i.e., as $\log_{10}(\tau_K)$ versus T_g/T. Keeping in mind that the viscosity η is proportional to τ up to a shear modulus at infinite frequency (a quantity which is known to vary slowly compared to the viscosity) one sees that, as expected, Fig. 5(c) displays the characteristic curvature of a semifragile glass-forming liquid.

Let us finally consider ω_{max}, the position of the α-peak maximum of $\chi''(\omega)$. ω_{max}^{-1} is proportional to τ_α, which is predicted to obey Eq. (2.9). A fit gave $\gamma=3.17$ and $T_c^{\alpha 1}=273\,°C$ as best fit parameters and is shown by the solid circles in Fig. 5(d). The value of $T_c^{\alpha 1}$ is not unreasonable. It is within the supercooled phase, even

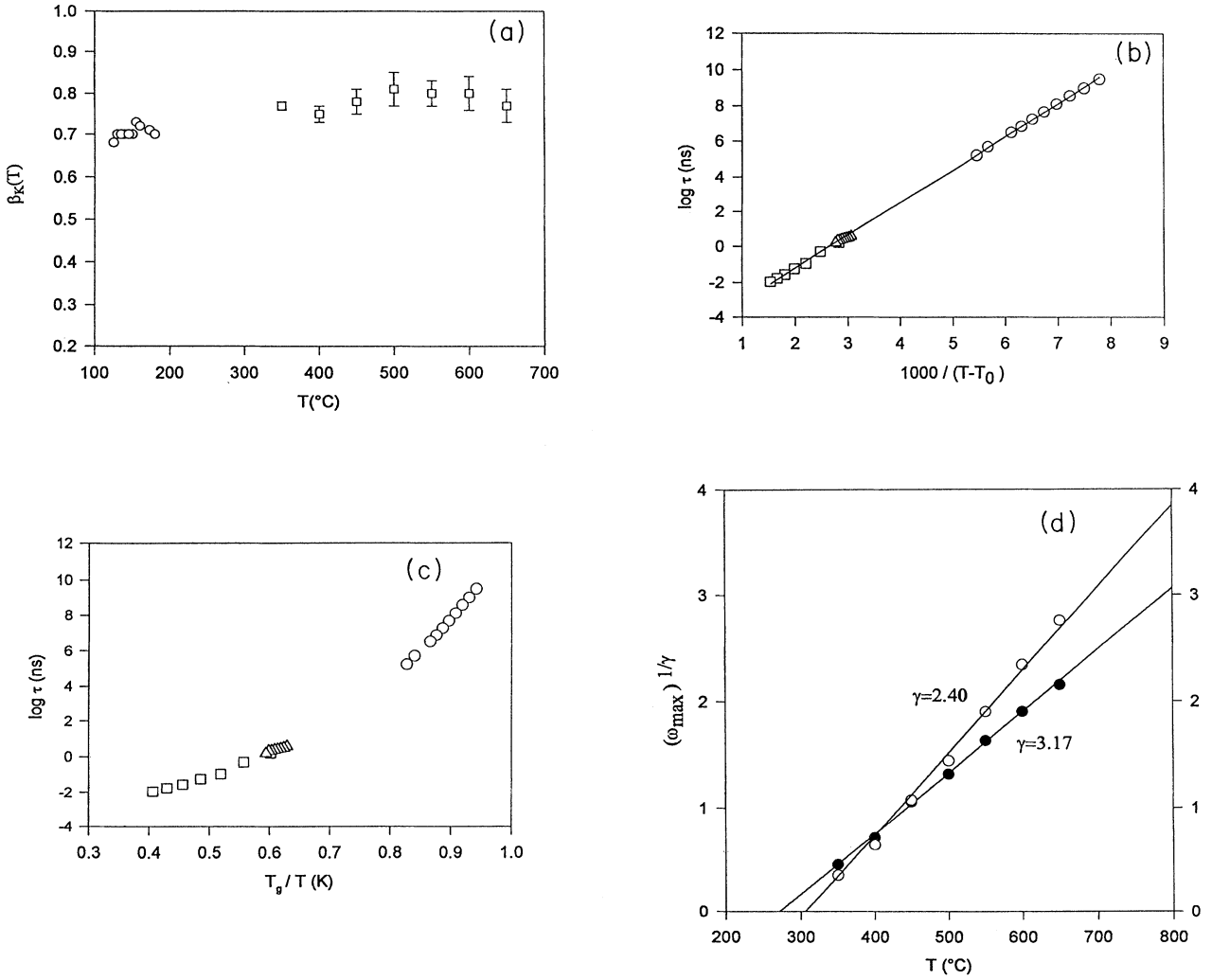

FIG. 5. (a) Variation of the stretching exponent β_K for the α-relaxation process with temperature: depolarized light-scattering data (□), photon correlation data [18] (○). (b) Variation of the relaxation time τ_K with temperature on a Vogel-Fulcher plot with $T_0=1\,°C$. The coefficients of the Vogel-Fulcher law were obtained by fitting simultaneously the depolarized light-scattering data (□) together with viscosity (△) [5] and photon correlation [18] (○) data. (c) Same data as in (b) plotted versus T_g/T. (d) Variation of $(\omega_{max})^{1/\gamma}$ with temperature. (●): $\gamma=3.17$, $T_c^{\alpha 1}=273\,°C$, (○): $\gamma=2.4$, $T_c^{\alpha 2}=306\,°C$.

TABLE I. Kohlrausch values of β_K and τ_K obtained from a fit to the α-relaxation process of the susceptibility spectra. The values obtained from a fit to a Cole-Davidson function have been transformed into a Kohlrausch function according to [39]. Values obtained from the combination of viscosity [5,6] and acoustic measurements [17] are indicated by an asterisk.

T (°C)	$\tau(ns)$	β
323.2	3.76*	1
328.1	3.12*	1
333	2.86*	1
338	2.66*	1
342.8	2.43*	1
347.8	2.16*	1
350	1.59	0.77
352.8	2.08*	1
357.8	1.54*	1
400	0.50	0.75
450	0.11	0.78
500	0.057	0.81
550	0.028	0.80
600	0.017	0.80
650	0.011	0.77

though this temperature could not be observed because of the crystallization of the sample.

B. Region of the minimum

The region of the susceptibility minimum has been the object of several recent studies because, as already noted, the MCT makes general predictions for this region. For the fragile glasses, Salol [35], orthoterphenyl (OTP) [36], propylene carbonate [37], and CKN [2], good agreement was found between MCT power-law predictions and the experiments. Also, the interpolation Eq. (2.4) was found to yield a fairly good agreement in the minimum region for about 2.5 decades in frequency. This interpolation formula implies that there exists a scaling range for the susceptibility spectra.

We tried to fit our data by means of these equations using the following procedure. A first fit to Eq. (2.4) for each temperature with a and b free was used to extract the $\chi''_{\min}$ and $\omega_{\min}$. The values found for the four fitting parameters are listed in Table II. Although b is almost constant in the whole temperature range in the free fits, the coefficient a has a large variation and is always outside of the theoretical limits. A second, global, fit with a and b forced to be constant for the whole set of spectra was carried out next, and a scaling plot with $\chi''_{\min}$ and $\omega_{\min}$ is shown in Fig. 6. The fit is quite good at low frequencies and it describes the minimum in a narrow frequency range, but the agreement fails at high frequencies. Furthermore, the a and b values ($a=1.04$ and $b=0.57$) do not obey Eq. (2.7) or the inequality (2.8). A fit with a and b forced to be constant for the whole set of spectra and also constrained to obey Eq. (2.7) was attempted without success. Another prediction of MCT is the variation of the frequency of the minimum of $\chi''(\omega)$ with T [see Eq. (2.6)]. Because of the uncertainties in determining $\omega_{\min}$, the method turned out to be inconclusive: no set of parameters giving a sharp minimum in the statistical χ^2 could be found, and the values of a and T_c turned out to be strongly correlated. Therefore, a fit of Eq. (2.6) with $a=0.31$ [a value related to b by Eq. (2.7)] was performed, which yielded $T_c^{\beta}=215$ °C, as shown in Fig. 7.

TABLE II. $\chi''_{\min}$, $\omega_{\min}$, a and b obtained from fits to Eq. (2.4) of the experimental susceptibility spectra without constraints on a and b. Last two columns: values of $\chi''_{\min}$ and $\omega_{\min}$ for a and b fixed: $a=1.04$, $b=0.57$.

T (° C)	$\chi''_{\min}$	$\omega_{\min}$	a	b	$\chi''_{\min}$	$\omega_{\min}$
350	61.9	59.1	1.39	0.51	63.3	53.1
400	93.0	50.2	1.05	0.53	89.9	49.1
450	174.7	113.9	1.18	0.72	190.9	114.3
500	247.6	133.5	0.82	0.72	250.6	144.0
550	347.6	182.2	0.70	0.66	340.0	185.4
600	442.5	238.7	0.74	0.65	438.6	239.0
650	599.8	3082	0.87	0.58	599.3	289.1

The reason why the idealized MCT does not give satisfactory agreement with the experiment can be seen clearly in Fig. 6. At low temperatures, the region above the susceptibility minimum is severely perturbed by the boson peak, which, being a part of the LSE, has a stronger intensity for a stronger glass former like $ZnCl_2$. In order to extract from the susceptibility spectrum the part relevant to MCT, Fujara and Petry [38] proposed the following procedure: by cooling down the glass former (tri-α-naphtylbenzene) below T_g, they determined the vibrational part of the susceptibility spectra, which can be identified here with the LSE structure described at the beginning of this section. Assuming that this vibrational profile does not vary with temperature, they subtracted it from the total susceptibility at higher temperature and thus extracted the part relevant for MCT. In our case, the result of this procedure turned out to be disappoint-

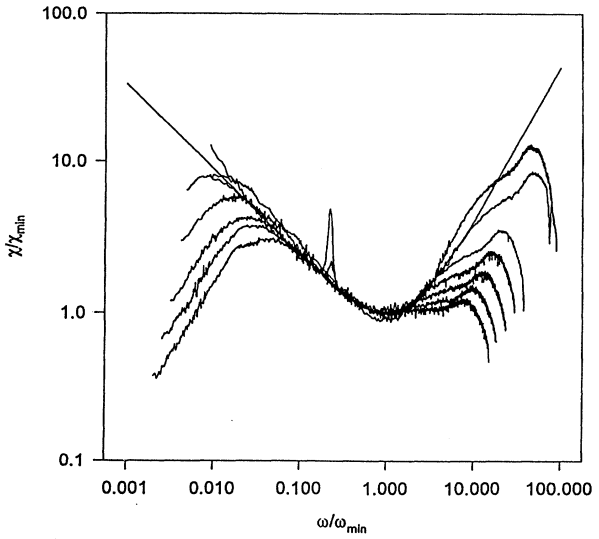

FIG. 6. Rescaled experimental susceptibility spectra and best global fit (——) to Eq. (2.4) with $a=1.04$ and $b=0.57$.

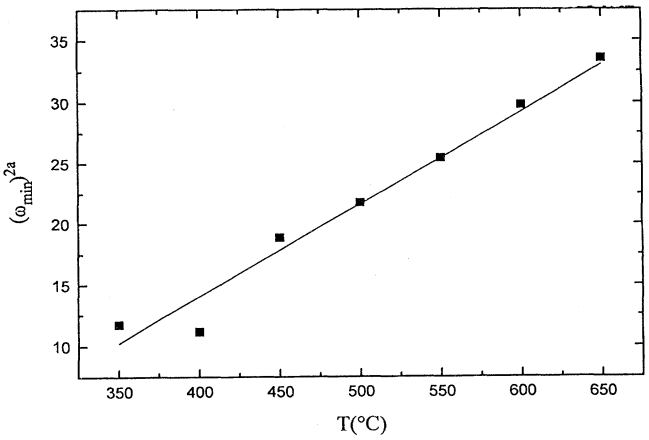

FIG. 7. Variation of $(\omega_{min})^{2a}$ with temperature taking $a=0.31$. The solid line is a linear fit yielding $T_c^{\beta}=215\,°C$.

ing. After subtraction we obtained a very weak residual susceptibility, much weaker than the vibrational part determined at the lower temperature (300 °C) and therefore very sensitive to the exact shape of this vibrational part [39].

However, since the von Schweidler part of the minimum is never severely disturbed by the boson peak, b is well determined from the global fit shown in Fig. 6 ($b=0.57$) and one can check whether the MCT predictions concerning the link between this region and the α peak hold. Assuming Eq. (2.7) to be valid, this yields $\gamma=2.4$, which is different from the value of the best fit made on ω_{max} [see Fig. 5(d)]. Another fit was carried out on ω_{max} with γ fixed at 2.4, which yielded $T_c^{\alpha 2}=306\,°C$, a temperature which, as $T_c^{\alpha 1}$, corresponds to the supercooled phase. This fit is also shown in Fig. 5(d) (open circles) and appears to be still reasonable.

C. The LSE region

Let us consider now the behavior of the high-frequency (or LSE) region. Figures 3(a) and 3(b) show that it contains: (i) above 2000 GHz, a peak, the frequency and shape of which do not appreciably change with temperature; (ii) a lower-frequency shoulder, quite apparent around 500 GHz in the low temperature spectra, with strong temperature dependence.

In order to explore the behavior of this second feature, we have performed, following methods introduced, e.g., in Refs. [40] or [41], a simple phenomenological analysis of the susceptibility spectra, assuming that they can be approximated by the sum of two Lorentzians and the α-relaxation process already analyzed. The frequency and width [half width at half maximum (HWHM)] of the high-frequency Lorentzian were assumed to be temperature independent, while its intensity, as well as the three parameters of the lower-frequency Lorentzian were allowed to vary with temperature. The α-relaxation process was described by the Cole-Davidson function using the τ and β parameters determined in Sec. IV A, while its intensity was used as an additional fitting parameter at each temperature.

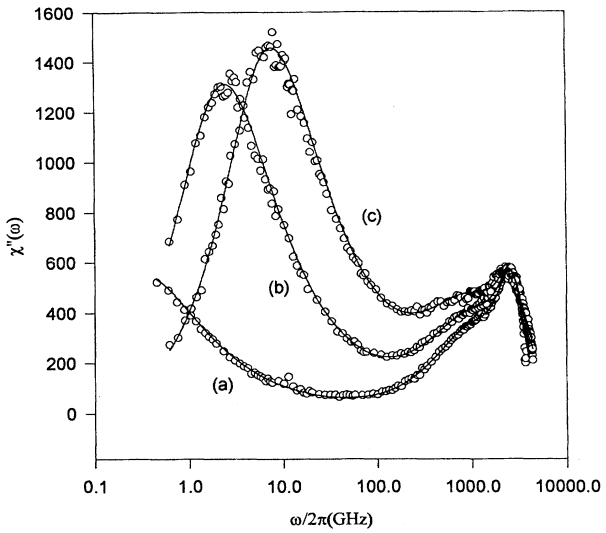

FIG. 8. Global fit of susceptibility spectra for the whole frequency range: (a) 400 °C, (b) 500 °C, (c) 600 °C.

The global fit obtained with this procedure is shown in Fig. 8 for three different temperatures, the three contributions to the fit for $T=500\,°C$ are illustrated in Fig. 9, and the parameters found from the fits are listed in Table III. Altogether this fit is satisfactory. The maximum of the high-frequency Lorentzian approximately coincides with a vibrational structure also seen in the Raman spectrum of the crystal δ phase [13]. This explains the term "microscopic peak" that we have used to describe it.

Figure 10 shows that, while the width Γ_B of the lower-frequency peak has only a small increase with increasing temperature, its frequency ω_B decreases sharply around 500 °C and is effectively equal to zero above this temperature. In agreement with recent measurements,

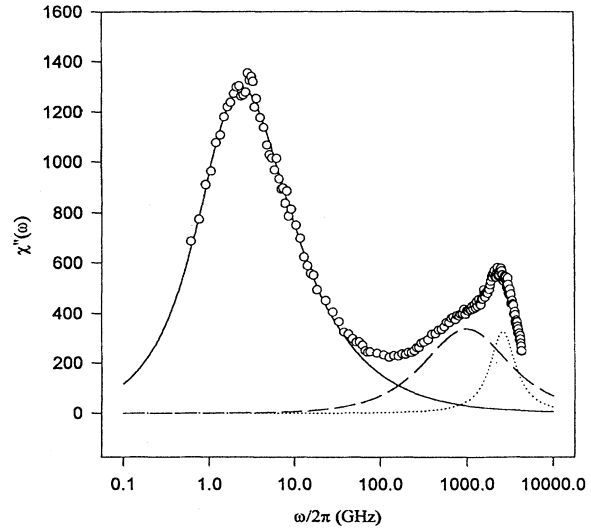

FIG. 9. Contribution to the susceptibility spectrum of Fig. 8 for $T=500\,°C$: α-relaxation process (——), boson peak (— — —), and microscopic peak (· · · ·).

TABLE III. Frequency (ω), HWHM (Γ), and relative intensities of the microscopic peak (m), bosonpeak (B), and α-relaxation process (α) from a phenomenological analysis of the susceptibility spectra, described in the text as illustrated in Fig. 9.

T (° C)	ω_m (GHz)	Γ_m (GHz)	ω_B (GHz)	Γ_B (GHz)	I_B/I_m	I_α/I_m *10^3
300	2370	1050	540	790	1.1	
320	2370	1050	480	860	1.4	
350	2370	1050	430	890	1.6	12
400	2370	1050	210	940	2.6	8
450	2370	1050	280	940	2.6	18
500	2370	1050	0	980	4.8	21
550	2370	1050	0	950	5.8	23
600	2370	1050	0	970	6.2	27
650	2370	1050	0	1040	6.3	31

which reported a similar behavior for the boson peak in some fragile and less fragile glasses [42], we have called this second contribution to the LSE the boson peak.

Let us finally point out that (i) the boson peak is always very broad, its width (HWHM) being always larger than its frequency; (ii) at 500 °C and above, the α-relaxation process still gives an appreciable contribution to the susceptibility spectra around 100 GHz, i.e., in a region dominated by the boson peak, although ω_{max} is smaller than ω_B by more than one order of magnitude.

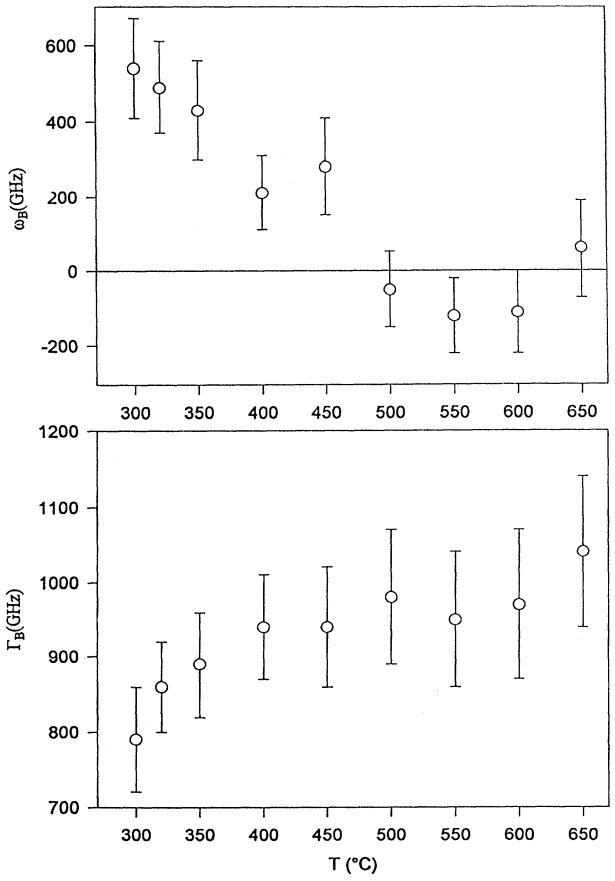

FIG. 10. Frequency ω_B and linewidth (HWHM) Γ_B of the boson peak versus temperature from the fits shown in Figs. 8 and 9. (Note that above 450 °C, due to the large error bars, ω_B is listed as 0 in Table III).

V. DISCUSSION

The preceding results can be analyzed from two different points of view.

A. Mode coupling theory

(i) Because of the existence of a strong boson peak in our depolarized spectra, we have not been able to test MCT properly in the region of the minimum of the susceptibility, the region for which the experiments on fragile glass formers were found to agree with the theoretical predictions. In particular, the T_c^β value obtained from the fit shown in Fig. 7 is not reliable because the frequency of the minimum cannot be properly determined. However, there are predictions of MCT that survive in the experiment; in particular, it has been recognized [3(c)] that a signature of the existence of a β-relaxation regime should be a difference between the b coefficient, which characterizes the von Schweidler regime of the α relaxation and the exponent β_K of the stretched exponential. In the present case, both β_K and b are temperature independent and we find $\beta_K=0.75$ and $b=0.57$. The difference between the two coefficients is of the same sign and order of magnitude that has been found for fragile liquids such as orthoterphenyl ($0.8<\beta_K<0.95$, $b=0.65$) [36], Salol ($\beta_K=0.58$, $b=0.41$) [35], or CKN ($\beta_K=0.58$, $b=0.41$) [2]. (ii) We have found, by analyzing the thermal evolution of τ_α, that T_c is much larger than T_g, the most reliable estimate being between 270 °C and 310 °C. The corresponding value for T_c/T_g is much larger (approximately 1.5) than the value generally reported for fragile glass-former liquids. This result can be correlated with the following observation: when a glass-former liquid is analyzed following the MCT technique, its T_c is found to be close to the crossing point, on an Angell plot, between the high and low temperature tangents to the viscosity curve. For less fragile glass formers such as $ZnCl_2$, the crossing point occurs at a considerably smaller value of T_g/T, e.g., a higher temperature relative to T_g. Nevertheless, the T_c estimate given here should be treated with caution: even though the temperature range in which Eq. (2.9) was found to be fulfilled is quite large, there is no means to check whether the range where this equation is applicable extends below 340 °C, the temperature down to which we analyzed ω_{max}.

We can summarize this MCT analysis of our data by stating that the values $T_c=290\,°C\pm20\,°C$ and $b\approx0.57$ are consistent with our light-scattering experiments. However, the MCT predictions for the detailed structure of the susceptibility minimum and the existence of a fast β-relaxation process could neither be substantiated nor ruled out by our results.

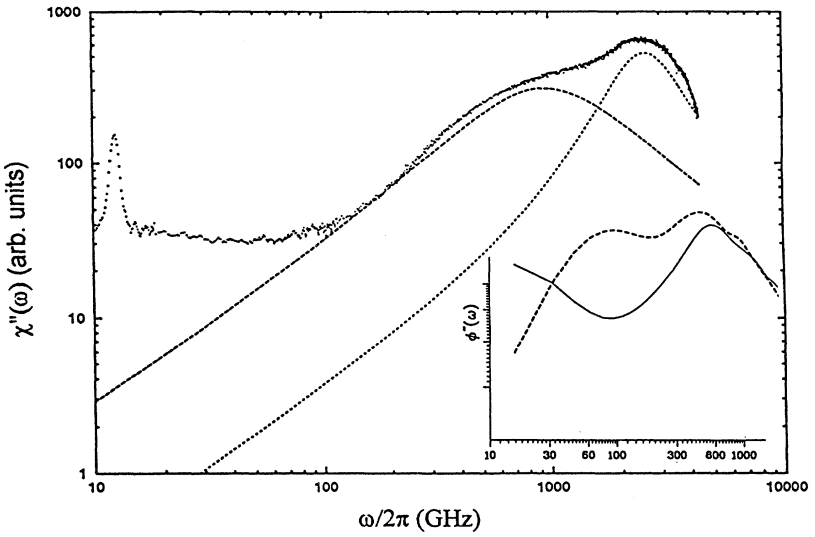

FIG. 11. Comparisons between the experimental boson peak obtained by depolarized light scattering and molecular dynamics results [47]. Experimental susceptibility spectrum at 320 °C, boson peak (— — —), and microscopic peak (· · · ·). Inset: susceptibility spectrum obtained by molecular dynamics for a Cl^- self-correlation function for $q=0.21$ $Å^{-1}$ at different temperatures: $T=327$ °C, (— — —); $T=177$ °C, (——).

B. The boson peak

The origin of a boson peak in the Raman spectra of glasses has been the subject of much controversy. Martin and Brenig [43] proposed that the origin of this peak is the modification of the light-scattering mechanism for large wave-vector acoustic modes by the medium-range order of the glass. More recent heat capacity and incoherent inelastic neutron-scattering measurements [44] as well as molecular dynamics (MD) [45] calculations showed the existence of an additional density of states in the same frequency range. In particular, those MD calculations showed that these low-frequency modes are quite localized, involve a small number of particles, and correspond to small amplitude vibrations. This should result in a contribution to the inelastic incoherent neutron dynamical structure factor $S(q,\omega)$, the intensity of which should increase proportionally to q^2. This effect has been observed by Buchenau in some polycarbonates [46]. A recent MD calculation of the liquid phase of $ZnCl_2$ performed by Foley, Wilson, and Madden [47] shows the existence of such a peak in the partial Cl^- self-correlation structure factor, the intensity of which also scales with q^2. In Fig. 11, we show the experimental boson peak just above the melting point and Cl^- self-correlation susceptibility spectra from MD for two temperatures. Though the Foley, Wilson, and Madden results do not yield a very accurate description of molten $ZnCl_2$ (in particular, their α relaxation is too fast and their T_g is too low), MD and experimental results are sufficiently close to give strong support to the idea that the boson peak we measure in our depolarized light-scattering spectra is connected with the existence of a low-frequency density of localized states in the molten salt, the peak frequency of which decreases with increasing temperature.

Such an evolution has also been reported by Sokolov *et al.* [42] in two fragile glass formers: orthoterphenyl and meta-tricresyl-phosphate, as well as in the intermediate glass former glycerol, with an approach different from the one used here. These authors define a temperature dependent frequency related to the boson peak, which extrapolates to zero for a temperature T^* approximately equal to T_c. This is not the case here; we find that the frequency of the boson peak in $ZnCl_2$ approaches zero for $T^* \approx 500$ °C; e.g., some 200 °C above the probable region of T_c.

These findings offer a real challenge to MCT. The modes appearing in the boson peak are strongly temperature dependent and extend to very low frequencies. Since they have not been included in the current formulation of MCT, their possible influence on the behavior of the susceptibility minimum is unknown and should be explored.

ACKNOWLEDGMENTS

We gratefully acknowledge P. Madden and G. Fytas for communicating their results prior to publication. We also acknowledge J. Vagner and the Département de Recherches Physiques workshop for the building of the oven, J. Toulouse for his early participation in this experiment, W. Götze for helpful discussion and suggestions, J. P. François for the preparation of the $ZnCl_2$ samples, and M. Albrecht for his help during the modification of the optical setup. H.Z.C. thanks the DRP and Université Pierre and Marie Curie for hospitality and financial support. M.J.L. acknowledges partial financial support from Saint-Gobain Recherches. Work at City College was supported by National Science Foundation Grant No. DMR 9315526. This study was partly supported by NATO Grant No. CRG-930730.

[1] (a) M. Kiebel, E. Bartsch, O. Debry, F. Fujara, W. Petry, and H. Sillescu, Phys. Rev. B **45**, 10 301 (1992); (b) F. Mezei, W. Knaak, and B. Farago, Phys. Rev. Lett. **58**, 571 (1987); (c) Europhys. Lett. **7**, 529 (1988).
[2] G. Li, W. M. Du, X. K. Chen, H. Z. Cummins, and N. J. Tao, Phys. Rev. A **45**, 3867 (1992).
[3] (a) U. Bengtzelius, W. Götze, and A. Sjölander, J. Phys. C **17**, 5915 (1984); (b) E. Leutheusser, Phys. Rev. A **29**, 2765 (1984); (c) W. Götze and L. Sjögren, Rep. Prog. Phys. **55**, 241 (1992).
[4] (a) J. Wüttke, J. Hernandez, G. Coddens, G. Li, H. Z. Cummins, F. Fujara, W. Petry, and H. Sillescu, Phys. Rev. Lett. **72**, 3052 (1994); (b) E. Rössler, A. P. Sokolov, A. Kisliuk, and D. Quitmann, Phys. Rev. B **49**, 14 967 (1994).
[5] J. D. Mackenzie and W. K. Murphy, J. Chem. Phys. **33**, 366 (1960).
[6] A. J. Easteal and C. A. Angell, J. Chem. Phys. **56**, 4231 (1972).
[7] C. A. Angell, in *Relaxation in Complex Systems,* edited by K. L. Ngai and G. B. Wright, National Research Laboratory, Washington, DC (1984), p. 3.
[8] R. Triolo and N. H. Narten, J. Chem. Phys. **74**, 703 (1981).
[9] S. Biggin and J. E. Enderby, J. Phys. C. **14**, 3129 (1981).
[10] J. A. E. Desa, A. C. Wright, J. Wong, and R. N. Sinclair, J. Non-Cryst. Solids **51**, 57 (1982).
[11] D. A. Allen, R. A. Howe and N. D. Wood, J. Chem. Phys. **94**, 5071 (1991).
[12] J. Wong and F. W. Lytle, J. Non-Cryst. Solids **8**, 376 (1974).
[13] F. Aliotta, G. Maisano, P. Migliardo, C. Vasi, F. Wanderlingh, G. Pedro-Smith, and R. Triolo, J. Chem. Phys. **75**, 613 (1981); M. L. Cacciola, S. Magazù, P. Migliardo, F. Aliotta, and C. Vasi, Solid State Commun. **57**, 125 (1969).
[14] C. A. Angell and J. Wong, J. Chem. Phys. **53**, 2053 (1970); C. A. Angell, J. Am. Soc. **51**, 125 (1969).
[15] H. E. Gunilla Knape, J. Chem. Phys. **80**, 4788 (1984).
[16] M. Soltwisch, J. Sukmanovski, and D. Quitmann, J. Chem. Phys. **86**, 3207 (1987).
[17] G. S. Gruber and T. A. Litovitz, J. Chem. Phys. **40**, 13 (1964).
[18] E.A. Pavlatou, G. N. Papatheodorou, and G. Fytas (unpublished); E. A. Pavlatou, Ph. D. thesis, University of Patras, 1994 (unpublished).
[19] V. K. Malinovski and A. P. Sokolov, Solid State Commun. **57**, 757 (1986).
[20] A. P. Sokolov, E. Rössler, A. Kisliuk, and D. Quitmann, Phys. Rev. Lett. **71**, 2062 (1993).
[21] K. Kawasaki, Ann. Phys. (N.Y.) **61**, 1 (1970).
[22] W. Götze and L. Sjögren, J. Phys. Condens. Matter **1**, 4183 (1989).
[23] W. Götze and L. Sjögren, Z. Phys. B **65**, 415 (1987); J. Phys. C. **21**, 3407 (1988).
[24] B. Berne and R. Pecora, *Dynamic Light Scattering* (Wiley, New York, 1976); J. P. Boon and S. Yip, *Molecular Hydrodynamics* (McGraw-Hill, New York, 1980).
[25] *Phenomena Induced by Molecular Interactions,* edited by G. Birnbaum (Plenum, New York, 1985), Series B, Vol. 127.
[26] P. A. Madden, Mol. Phys. **36**, 365 (1978).
[27] M. J. Stephen, Phys. Rev. **187**, 279 (1969).
[28] A. Bikhovskii and R. M. Pick, J. Chem. Phys. **100**, 7109 (1994).
[29] N. J. Tao, G. Li, X. Chen, W. M. Du, and H. Z. Cummins, Phys. Rev. A **44**, 6665 (1991).
[30] J. R. Tessman, A. H. Kahn, and W. Shockley, Phys. Rev. **92**, 890 (1953).
[31] P. A. Madden, K. O'Sullivan, J. A. Board, and P. W. Fowler, J. Chem. Phys. **94**, 918 (1991).
[32] R. Mok, B. Hillebrands, and J. R. Sandercock, J. Phys. E **20**, 656 (1991).
[33] C. Alba-Simionesco and M. Krauzman, J. Chem. Phys. (to be published).
[34] C. P. Lindsey and G. D. Paterson, J. Chem. Phys. **73**, 3348 (1980).
[35] G. Li, W. M. Du, A. Sakai, and H. Z. Cummins, Phys. Rev. A **46**, 3343 (1992).
[36] W. Steffen, A. Patkowski, H. Glaser, G. Meier, and E. W. Fischer, Phys. Rev. E **49**, 2992 (1994).
[37] W. M. Du, G. Li, H. Z. Cummins, M. Fuchs, J. Toulouse, and L. A. Knauss, Phys. Rev. E **49**, 2192 (1994).
[38] F. Fujara and W. Petry, Europhys. Lett. **4**, 921 (1987).
[39] Note that a similar result was obtained for glycerol in [4b].
[40] D. Kivelson, X. C. Zeng, H. Sakai, and G. Tarjus, J. Mol. Struct. (to be published).
[41] A. Patkowski, W. Steffen, G. Meier, and E. W. Fischer, J. Non-Cryst. Solids, **172**, 52 (1994).
[42] A. P. Sokolov, A. Kisliuk, D. Quitmann, A. Kudlick, and E. Rössler, J. Non-Cryst. Solids **172**, 113 (1994).
[43] A. J. Martin and W. Brenig, Phys. Status Solidi B **64**, 163 (1974).
[44] U. Buchenau, Philos. Mag. B **65**, 303 (1992).
[45] B. B. Laird and H. R. Schober, Phys. Rev. Lett. **66**, 636 (1991).
[46] U. Buchenau (unpublished).
[47] M. Foley, M. Wilson, and P. A. Madden (unpublished).